# ChemComm

## COMMUNICATION

Check for updates

# AIE-active iridium(III) complex integrated with upconversion nanoparticles for NIR-irradiated photodynamic therapy†

Shengnan Liu, [‡a] Jiahong Han,[‡a] Yulei Chang, [*b] Weijin Wang,[a] Runlin Wang,[a] Ziwei Wang,[a] Guangzhe Li,[*c] Dongxia Zhu [*a] and Martin R. Bryce [*d]

The integration of an aggregation induced emission (AIE)-active Ir(III) complex and upconversion nanoparticles (UCNPs) has achieved a NIR-irradiated photosensitizer (PS), UCNPs@Ir-2-N. This PS has satisfactory biocompatibility, excellent phototoxicity, good accumulation in cells and high $^1O_2$ generation ability, thereby effectively killing 4T1 mouse cancer cells *in vitro*. This work has potential for future photodynamic therapy (PDT) applications.

Photodynamic therapy (PDT) is an efficient anticancer treatment of particular interest.[1–3] In the PDT process light irradiates photosensitizers (PSs) to generate highly cytotoxic reactive oxygen species (ROS) causing the ablation of cancer cells.[4–6] Traditional PSs suffer from several major drawbacks:[7–10] (i) low intersystem crossing (ISC) ability; (ii) poor photostability; (iii) aggregation-caused quenching (ACQ) of emission; (iv) unsatisfactory ROS production efficiency. Moreover, the short-wavelength irradiation light results in shallow tissue penetration and photodamage to cells and tissue.[11–13] Hence, the clinical application of PDT requires a solution to these problems.

Tang and co-authors have recently reported that aggregation-induced emission (AIE) luminogens show excellent aggregation-induced ROS generation activity.[14] However, how to make the most of accelerating the ISC process to boost ROS generation

still remains a key challenge. Inspired by the above facts, a few AIE-active Ir(III) complexes with efficient ISC processes, long excited-state lifetime, excellent photostability and tunable ligand modification have been developed as substitutes to traditional materials for efficient PDT.[7,15–18]

Nevertheless, the absorption bands of Ir(III) complexes are usually in the UV to visible range and not in the near-infrared (NIR) region,[19,20] which limits their therapeutic effect in deep tissue. Upconversion nanoparticles (UCNPs) are desirable photoconversion materials for biosensing and biomedicine on account of their capability of transforming the NIR photons to UV/visible photons.[11,13,21] Two reports have corroborated that PSs combining cationic Ir(III) complexes and UCNPs can overcome the problems caused by short wavelength irradiation in PDT.[22,23] Possibly owing to the lack of a reliable molecular design strategy or facile synthetic routes, to the best of our knowledge, there have not been any reports of PSs based on AIE-active Ir(III) complexes and UCNPs.

Herein, AIE-active non-charged Ir(III) complexes integrated with UCNPs are employed as effective PSs for PDT for the first time. Taking advantage of the tunable ligand structure of Ir(III) complexes,[24] a Schiff base was introduced as the ancillary N^O ligand due to its simple synthesis, high yield and proven coordination to achieve AIE-active Ir(III) complexes,[16,25] giving **Ir-1-N** (structure in ESI†) and **Ir-2-N** (Scheme 1). Compared with **Ir-1-N**, the absorption of **Ir-2-N** was extensively enhanced through extending the π-conjugation of the C^N ligands. Furthermore, **Ir-2-N** exhibits bright luminescence in the aggregated state and high singlet oxygen ($^1O_2$) generation ability. The **UCNPs@Ir-2-N** nanoparticles (NPs) were formulated by encapsulating the **Ir-2-N** and UCNPs within D-α-tocopherol polyethylene glycol 1000 succinate (TPGS) to obtain better stability and biocompatibility. **UCNPs@Ir-2-N** is the main focus of the current study.

The synthetic routes to **Ir-1-N** and **Ir-2-N** are shown in the ESI.† Their structures were validated by proton nuclear magnetic resonance ($^1H$ NMR) spectroscopy (Fig. S1–S6, ESI†),

[a] Key Laboratory of Nanobiosensing and Nanobioanalysis at Universities of Jilin Province, Department of Chemistry, Northeast Normal University, 5268 Renmin Street, Changchun, Jilin Province 130024, P. R. China.
E-mail: zhudx047@nenu.edu.cn

[b] State Key Laboratory of Luminescence and Applications, Changchun Institute of Optics, Fine Mechanics and Physics, Chinese Academy of Sciences, Changchun, Jilin Province 130033, China. E-mail: yuleichang@ciomp.ac.cn

[c] Jilin Provincial Science and Technology Innovation Center of Health Food of Chinese Medicine, Changchun University of Chinese Medicine, Changchun, Jilin Province 130117, P. R. China. E-mail: 1993008106@qq.com

[d] Department of Chemistry, Durham University, Durham, DH1 3LE, UK.
E-mail: m.r.bryce@durham.ac.uk

† Electronic supplementary information (ESI) available: Experimental details, supporting figures and tables. See DOI: https://doi.org/10.1039/d2cc03622c
‡ The authors contributed equally to the preparation of this work.
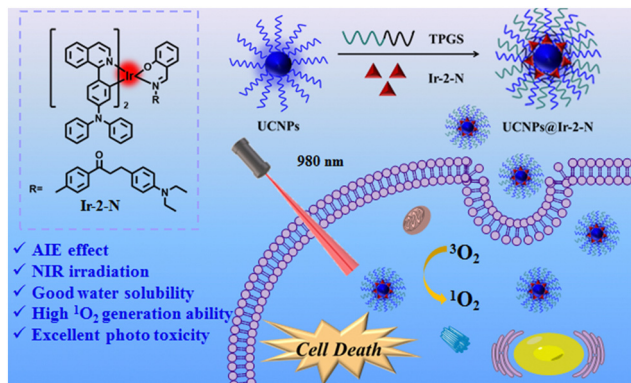
Scheme 1 Structure of **Ir-2-N**, preparation of **UCNPs@Ir-2-N** and schematic of **UCNPs@Ir-2-N** as a PS for PDT.

^{13}C NMR spectroscopy (Fig. S7 and S8, ESI†) and high-resolution mass spectrometry (HRMS) (Fig. S9 and S10, ESI†). The UCNPs (NaYF$_4$@NaF:Yb,Tm@NaYF$_4$) were prepared by the chloride solvothermal method as reported before[26] (see ESI†).

The photophysical properties of **Ir-1-N** and **Ir-2-N** were investigated (Fig. 1a and Fig. S11, Table S1, ESI†). In UV-vis absorption spectra, both of the Ir(III) complexes showed two absorption bands at 250–350 nm, corresponding to spin-allowed π–π* transitions at the ligand centers, and at 350–500 nm from metal-to-ligand charge transfer ([1]MLCT), ligand-to-ligand charge transfer ([1]LLCT), spin-forbidden metal-to-ligand charge-transfer ([3]MLCT) and spin-forbidden ligand-to-ligand charge-transfer ([3]LLCT).[19,27,28] The photoluminescence (PL) spectra show that **Ir-1-N** emits at $\lambda_{max}$ 640 nm, and **Ir-2-N** at 660 nm. These results establish that the extended conjugation of the C^N ligands leads

to a significant redshift in the PL of **Ir-2-N** and almost 1.5 times increase of the molar absorption coefficient of **Ir-2-N** relative to **Ir-1-N**. Moreover, these Ir(III) complexes are almost non-emissive in pure CH$_3$CN (Fig. 1b and Fig. S12, ESI†). On the contrary, the emission intensity of **Ir-1-N** and **Ir-2-N** was greatly enhanced when the water fraction reached respectively to 80% and 50% demonstrating their typical AIE feature. **Ir-2-N** showed a brighter luminescence indicating the effective restriction of nonradiative transition processes, as found in AIE luminogens.[29–31] Meanwhile, there are clear level-off tails at higher wavelengths in the UV-vis absorption spectra with the enhancement of water faction because of the Mie scattering effect from the aggregated suspensions[32] (Fig. S13, ESI†). Transmission electron microscopy (TEM) provided further evidence for molecular aggregates of **Ir-1-N** and **Ir-2-N** in the 99% H$_2$O/CH$_3$CN mixture (Fig. S14, ESI†). Both complexes **Ir-1-N** and **Ir-2-N** exhibited a long excited-state lifetime of 0.56 μs and 0.62 μs, respectively, and high photoluminescence quantum yield (PLQY) of nearly 20% in the aggregated state (Table S1, ESI†).

In view of the promising optical properties of **Ir-1-N** and **Ir-2-N**, their PDT applications were investigated. Indocyanine green (ICG), for which the absorption band at 790 nm will decrease after encountering [1]O$_2$, was utilized as a [1]O$_2$ generation indicator.[7] In Fig. S15 (ESI†), the absorption of ICG shows negligible change in the control groups. And there are also no changes in the absorption of the Ir(III) complexes upon irradiation (425 nm, 20 mW cm$^{-2}$) implying their good photostability. In contrast, the absorption of ICG at 790 nm rapidly decreased in intensity under 425 nm light irradiation in the presence of 15 μg mL$^{-1}$ of **Ir-2-N**. However, irradiating the **Ir-1-N** solution at the same concentration did not bring a significant change of the spectra (Fig. S15c and d, ESI†). Fig. 1d illustrates that the [1]O$_2$ generation of the complexes follows first-order kinetics and the slope of **Ir-2-N** is much higher than that of **Ir-1-N**, suggesting the higher [1]O$_2$ generation ability of **Ir-2-N**, which could originate from the higher absorption coefficient of **Ir-2-N**.[33] The NPs of **Ir-1-N** and **Ir-2-N** (**Ir-1-N NPs** and **Ir-2-N NPs**) were self-assembled with poloxamer (F127) (ESI†), and their [1]O$_2$ generation ability was obviously enhanced compared to **Ir-1-N** and **Ir-2-N** (Fig. 1c, d and Fig. S16, ESI†). This enhancement is attributed to the AIE features of the Ir(III) complexes. Contemporaneously, **Ir-2-N NPs** exhibited higher [1]O$_2$ generation ability due to its stronger AIE features compared to **Ir-1-N NPs**, meaning **Ir-2-N** has the capacity to be utilized as a PS in the aggregated state. Therefore, **Ir-2-N** was used for subsequent experiments.

To overcome the drawbacks of the short wavelength absorption bands, **Ir-2-N** and UCNPs were integrated to improve the PS performance. **Ir-2-N** was encapsulated with UCNPs within TPGS to construct **UCNPs@Ir-2-N** (see ESI†) as PSs for the ensuing *in vitro* experiments. A scanning electron microscope (SEM) image showed a uniform morphology and size of the UCNPs (Fig. S17, ESI†). TPGS not only enables the integration of **Ir-2-N** and UCNPs, but also increases the biocompatibility of NPs.[34] The UV-vis absorption spectra of **UCNPs@Ir-2-N** showed a significant absorption at about $\lambda_{max}$ 425 nm corresponding to that of **Ir-2-N** (Fig. 2a). Energy dispersive spectroscopy (EDS)
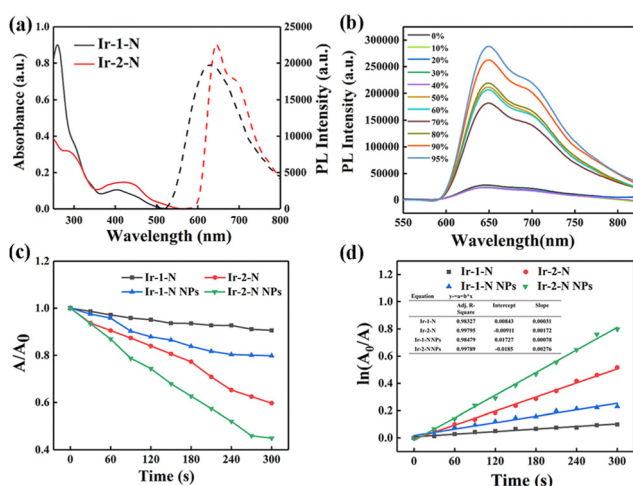


Fig. 1 (a) The UV–vis absorption spectra in CH$_3$CN (solid line) and the PL spectra in the mixed solvent (CH$_3$CN : H$_2$O = 1 : 9 v/v) of **Ir-1-N** and **Ir-2-N** (10$^{-5}$ M) (dashed line). (b) PL spectra of **Ir-2-N** in CH$_3$CN–H$_2$O mixtures (complex concentration = 1.0 × 10$^{-5}$ M) with different water fractions (0–95% v/v) at room temperature. (c) The decay rates of ICG in the presence of **Ir-1-N** and **Ir-2-N** and their **NPs** upon exposure to light (425 nm, 20 mW cm$^{-2}$). (d) Time-dependent [1]O$_2$ generation kinetics. $A_0$ = initial absorbance maximum of ICG. $A$ = real-time absorbance maximum of ICG with various light exposure times.
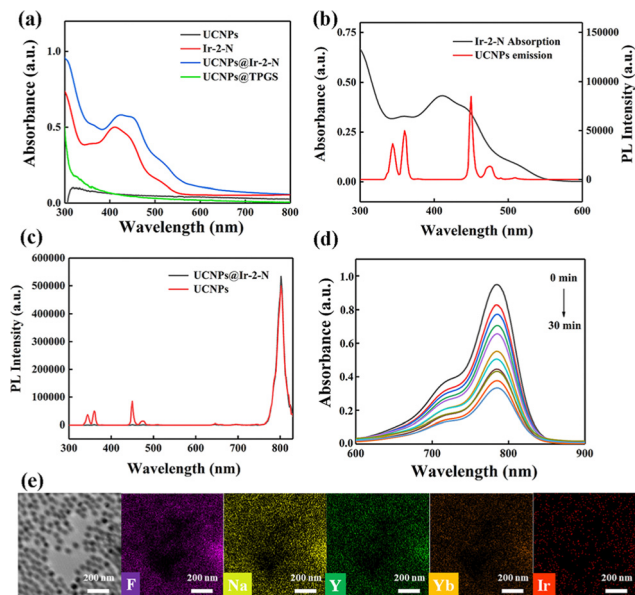
Fig. 2 (a) The UV-vis absorption spectra of **Ir-2-N**, **UCNPs**, **UCNPs@TPGS** and **UCNPs@Ir-2-N**. (b) The UV-vis absorption spectra of **Ir-2-N** (black line) and the PL spectra of UCNPs (red line). (c) The PL spectra of UCNPs and **UCNPs@Ir-2-N**. (d) The UV-vis absorption spectra of ICG (5 µg mL$^{-1}$) with **UCNPs@Ir-2-N** (15 µg mL$^{-1}$) under 980 nm irradiation. (e) The EDS mapping of **UCNPs@Ir-2-N**.

confirmed the even distribution of the elements: F, Na, Y, Yb, Ir in **UCNPs@Ir-2-N** (Fig. 2e). The loading content of **Ir-2-N** in **UCNPs@Ir-2-N** was calculated to be 70% according to UV-vis spectral analysis (Fig. S18, ESI†). The hydrodynamic size and polydispersity index (PDI) of **UCNPs@Ir-2-N** were 113 nm and 0.256, respectively, detected by dynamic light scattering (DLS) (Fig. S19a, ESI†). The TEM images imply the average size of **UCNPs@Ir-2-N** is around 100 nm. Furthermore, one-week monitoring of the size and PDI of **UCNPs@Ir-2-N** revealed its excellent stability (Fig. S19b, ESI†) and hence potential applicability in PDT.

To ensure that the energy transfer between **Ir-2-N** and UCNPs can be realized and **UCNPs@Ir-2-N** could be irradiated by NIR light, the PL spectrum of UCNPs was measured under laser irradiation (980 nm). The absorption band of **Ir-2-N** is in the UV and blue regions overlapping with the emission bands of UCNPs (Fig. 2b). Next, the PL spectra of original UCNPs and **UCNPs@Ir-2-N** were compared. As shown in Fig. 2c and Fig. S18 (ESI†), the 345, 360, 450 and 470 nm bands nearly disappeared, due to strong absorption by **Ir-2-N** via ULRET (upconversion luminescence resonance energy transfer). This process is a prerequisite to use **UCNPs@Ir-2-N** as a PS for PDT upon NIR light irradiation.

Subsequently, the $^1O_2$ generation ability of **UCNPs@Ir-2-N** was assessed through ICG as indicator. Compared with the control groups, the absorption bands of ICG decreased in **UCNPs@Ir-2-N** solution with increasing the irradiation time under 980 nm light (Fig. 2d and Fig. S21a, b, ESI†). The data reveal an effective process to generate $^1O_2$: (i) UCNPs absorb the NIR light at 980 nm and emit the UV/blue light which is

absorbed by **Ir-2-N**; (ii) **Ir-2-N** is then excited and undergoes energy transfer through $O_2$ to form $^1O_2$. The absorption of **UCNPs@Ir-2-N** remains unchanged under irradiation (980 nm) over the same period (30 min) confirming its desirable photostability (Fig. S21c, ESI†). The $^1O_2$ generation ability of UCNPs was tested as a control, which further confirmed that the good $^1O_2$ generation ability of **UCNPs@Ir-2-N** was mainly from the **Ir-2-N** excited by UCNPs (Fig. S21d, ESI†). Hence, it has been demonstrated that the NIR-irradiated PSs obtained by the combination of UCNPs and Ir(III) complexes could ameliorate the problems coming from the short wavelength absorption of the Ir(III) complexes.

Encouraged by the $^1O_2$ generation ability of NIR-irradiated **UCNPs@Ir-2-N**, their ability to kill cancer cells through PDT was investigated. *In vitro* photo-cytotoxicity experiments using **UCNPs@Ir-2-N** with concentrations from 0 to 15 µg mL$^{-1}$ (in terms of the calculated concentration of **Ir-2-N** in NPs, see ESI† for details) were evaluated against 4T1 mouse breast cancer cells *via* 3-(4,5-dimethylthiazol-2-yl)-2,5-diphenyltetrazolium bromide (MTT) assays (Fig. 3a). Without NIR irradiation, the >85% viability of 4T1 cells indicated **UCNPs@Ir-2-N** possess a satisfactory biocompatibility. After exposure to 980 nm laser irradiation, the viability of **UCNPs@Ir-2-N**-treated cells decreased to 9%, pointing to the considerable cytotoxicity of **UCNPs@Ir-2-N** (IC$_{50}$ value = 3.68 µg mL$^{-1}$). The same concentration of UCNPs was used to conduct MTT assays as a control experiment (Fig. S22, ESI†). The data suggested that only UCNPs have negligible phototoxicity to 4T1 cells. To further visually evaluate the therapeutic effect of **UCNPs@Ir-2-N**, a Calcein AM and propidium iodide (PI) co-staining assay was
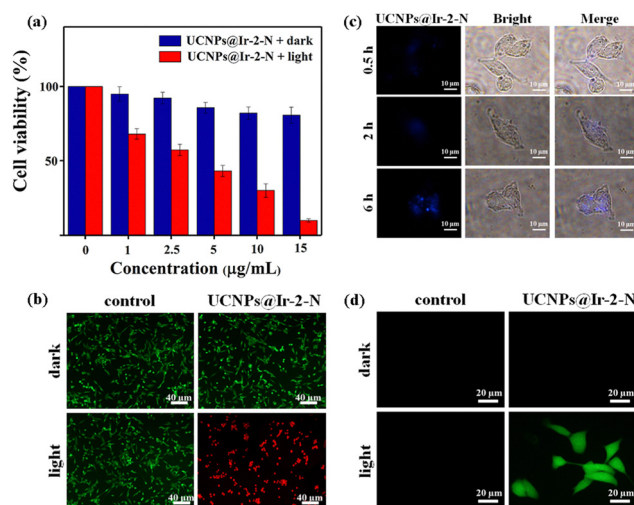


Fig. 3 (a) Relative viability of 4T1 cells after 24 h co-incubation with **UCNPs@Ir-2-N** under darkness and under irradiation (980 nm, 0.6 mW cm$^{-2}$). (b) Confocal fluorescence images of 4T1 cells co-stained with calcein-AM (live cells, green fluorescence) and propidium iodide (dead cells, red fluorescence) after treatment with **UCNPs@Ir-2-N** (15 µg mL$^{-1}$). (c) Cellular uptake of **UCNPs@Ir-2-N** (15 µg mL$^{-1}$) detected by CLSM at different periods of time. (d) Confocal fluorescence images for the detection of $^1O_2$ generation in 4T1 cells treated with **UCNPs@Ir-2-N** under irradiation (980 nm, 0.6 W cm$^{-2}$).

performed to stain viable and dead cells, respectively. There were negligible dead cells in control groups and the groups in dark conditions (Fig. 3b). In contrast, a majority of cells were dead in the group with **UCNPs@Ir-2-N** under 980 nm irradiation. This was in good accordance with the MTT assays. The data demonstrated that **UCNPs@Ir-2-N** could be employed as an NIR-irradiated PS and applied in efficient PDT.

The cellular uptake experiments further confirmed that **UCNPs@Ir-2-N** could be effectively ingested by 4T1 cells according to confocal laser scanning microscope (CLSM) imaging (Fig. 3c). The blue fluorescence signal (from the UCNPs in **UCNPs@Ir-2-N**) gradually enhanced with incubation time, implying a time-dependent uptake pathway and the efficient accumulation of **UCNPs@Ir-2-N** in cells. Furthermore, the *in situ* $^1O_2$ generation capability was evaluated using $2',7'$-dichlorofluorescein diacetate (DCFH-DA). As expected, **UCNPs@Ir-2-N**-treated cells exhibited strong green fluorescence under 980 nm irradiation, but almost no fluorescence was detected under dark conditions (Fig. 3d). The results are consistent with the fact that **Ir-2-N** could absorb the UV/blue light from NIR-irradiated **UCNPs** through ULRET and then generate $^1O_2$. All the results illustrate the feasible strategy that UCNPs and AIE-active **Ir-2-N** are encapsulated together to achieve effective energy transfer, and hence exert their respective advantages to construct NIR-irradiated PSs, **UCNPs@Ir-2-N** which generate toxic ROS and thereby kill the cancer cells. This approach has effectively overcome the problems of short-wavelength absorption of Ir(III) complexes.

In summary, two AIE-active Ir(III) complexes (**Ir-1-N** and **Ir-2-N**) were synthesized through rational molecular design. Extending the conjugation within the C^N ligands of **Ir-2-N** resulted in a redshift of its PL spectra and enhanced absorption. Moreover, **Ir-2-N** showed high $^1O_2$ generation ability and its AIE properties lead to increased $^1O_2$ generation in the aggregated state. **UCNPs** were applied as photoconversion materials to obtain **UCNPs@Ir-2-N**, in which ULRET between AIE-active **Ir-2-N** and UCNPs play a very important role under NIR irradiation. *In vitro*, NIR-irradiated **UCNPs@Ir-2-N** has satisfactory biocompatibility, excellent phototoxicity, good accumulation in cells and superior $^1O_2$ generation ability. To the best of our knowledge, this is the first report of PSs that combine AIE-active Ir(III) complexes with UCNPs. The work represents a significant development for PSs based on readily-available, high-performance transition metal complexes.

## Conflicts of interest

There are no conflicts to declare.

## Notes and references

1 D. W. Felsher, *Nat. Rev. Cancer*, 2003, **3**, 375–380.
2 T. Yan, L. Ren, F. Li, F. Tian, C. Jiang, Q. Wang, X. Song and S. Zhang, *Chem. Commun.*, 2022, **58**, 1617–1620.
3 X. Zhao, J. Liu, J. Fan, H. Chao and X. Peng, *Chem. Soc. Rev.*, 2021, **50**, 4185–4219.
4 L. Huang, S. Zhao, J. Wu, L. Yu, N. Singh, K. Yang, M. Lan, P. Wang and J. S. Kim, *Coord. Chem. Rev.*, 2021, **438**, 213888.
5 Z. Zhang, M. Kang, H. Tan, N. Song, M. Li, P. Xiao, D. Yan, L. Zhang, D. Wang and B. Z. Tang, *Chem. Soc. Rev.*, 2022, **51**, 1983–2030.
6 G. Jin, G. Feng, W. Qin, B. Z. Tang, B. Liu and K. Li, *Chem. Commun.*, 2016, **52**, 2752–2755.
7 L. Zhang, Y. Li, W. Che, D. Zhu, G. Li, Z. Xie, N. Song, S. Liu, B. Z. Tang, X. Liu, Z. Su and M. R. Bryce, *Adv. Sci.*, 2019, **6**, 1802050.
8 M. Liu, Y. Chen, Y. Guo, H. Yuan, T. Cui, S. Yao, S. Jin, H. Fan, C. Wang, R. Xie, W. He and Z. Guo, *Nat. Commun.*, 2022, **13**, 2179.
9 Y. Hong, J. W. Lam and B. Z. Tang, *Chem. Commun.*, 2009, 4332–4353.
10 J. Zhang, F. Fang, B. Liu, J. H. Tan, W. C. Chen, Z. Zhu, Y. Yuan, Y. Wan, X. Cui, S. Li, Q. X. Tong, J. Zhao, X. M. Meng and C. S. Lee, *ACS Appl. Mater. Interfaces*, 2019, **11**, 41051–41061.
11 Z. Wang, B. Liu, Q. Sun, L. Feng, F. He, P. Yang, S. Gai, Z. Quan and J. Lin, *ACS Nano*, 2021, **15**, 12342–12357.
12 P. S. Chelushkin, J. R. Shakirova, I. S. Kritchenkov, V. A. Baigildin and S. P. Tunik, *Dalton Trans.*, 2022, **51**, 1257–1280.
13 Y. Wang, Y. Li, Z. Zhang, L. Wang, D. Wang and B. Z. Tang, *Adv. Mater.*, 2021, **33**, 2103748.
14 Y. Li, R. Zhang, Q. Wan, R. Hu, Y. Ma, Z. Wang, J. Hou, W. Zhang and B. Z. Tang, *Adv. Sci.*, 2021, **8**, 2102561.
15 J. Liu, C. Jin, B. Yuan, X. Liu, Y. Chen, L. Ji and H. Chao, *Chem. Commun.*, 2017, **53**, 2052–2055.
16 L. Li, L. Zhang, X. Tong, Y. Li, Z. Yang, D. Zhu, Z. Su and Z. Xie, *Dalton Trans.*, 2020, **49**, 15332–15338.
17 D. Ding and B. Z. Tang, *Adv. Healthcare Mater.*, 2021, **10**, 2102499.
18 X. Cai, K. N. Wang, W. Ma, Y. Yang, G. Chen, H. Fu, C. Cui, Z. Yu and X. Wang, *J. Nanobiotechnol.*, 2021, **19**, 254.
19 Y. You and W. Nam, *Chem. Soc. Rev.*, 2012, **41**, 7061–7084.
20 G. Li, D. Zhu, X. Wang, Z. Su and M. R. Bryce, *Chem. Soc. Rev.*, 2020, **49**, 765–838.
21 Y. Feng, H. Chen, Y. Wu, I. Que, F. Tamburini, F. Baldazzi, Y. Chang and H. Zhang, *Biomaterials*, 2020, **230**, 119637.
22 J. Zhao, S. Sun, X. Li, W. Zhang and S. Gou, *ACS Appl. Bio Mater.*, 2020, **3**, 252–262.
23 J. Zhao, X. Zhang, L. Fang, C. Gao, C. Xu and S. Gou, *Small*, 2020, **16**, 2000363.
24 T. S. Teets, *ChemPhotoChem*, 2018, **2**, 380–381.
25 P. Ghosh, S. K. Dey, M. H. Ara, K. Karim and A. B. M. N. Islam, *Egypt. J. Chem.*, 2019, **62**, 523–547.
26 H.-S. Qian and Y. Zhang, *Langmuir*, 2008, **24**, 12123–12125.
27 C. You, D. Liu, J. Yu, H. Tan, M. Zhu, B. Zhang, Y. Liu, Y. Wang and W. Zhu, *Adv. Opt. Mater.*, 2020, **8**, 2000154.
28 H. F. Li, X. Q. Liu, C. Lyu, J. Gorbaciova, L. L. Wen, G. G. Shan, P. B. Wyatt, H. Q. Ye and W. P. Gillin, *Light: Sci. Appl.*, 2020, **9**, 32.
29 J. Luo, Z. Xie, J. W. Lam, L. Cheng, H. Chen, C. Qiu, H. S. Kwok, X. Zhan, Y. Liu, D. Zhu and B. Z. Tang, *Chem. Commun.*, 2001, 1740–1741.
30 J. Mei, Y. Hong, J. W. Lam, A. Qin, Y. Tang and B. Z. Tang, *Adv. Mater.*, 2014, **26**, 5429–5479.
31 F. Würthner, *Angew. Chem., Int. Ed.*, 2020, **59**, 14192–14196.
32 B. Xu, W. Li, J. He, S. Wu, Q. Zhu, Z. Yang, Y. C. Wu, Y. Zhang, C. Jin, P. Y. Lu, Z. Chi, S. Liu, J. Xu and M. R. Bryce, *Chem. Sci.*, 2016, **7**, 5307–5312.
33 X. Zheng, L. Wang, S. Liu, W. Zhang, F. Liu and Z. Xie, *Adv. Funct. Mater.*, 2018, **28**, 1706507.
34 T. Y. Lu, W. F. Lu, Y. H. Wang, M. Y. Liao, Y. Wei, Y. J. Fan, E. Y. Chuang and J. Yu, *ACS Appl. Mater. Interfaces*, 2021, **13**, 38074–38089.